Batteries & Supercaps

Research Article
doi.org/10.1002/batt.202500289

Chemistry Europe
European Chemical Societies Publishing

www.batteries-supercaps.org

A Long Cycle-Life and Recyclable Anthraquinone Oligomer Connected via Amide Bonds for Use in Rechargeable Organic Batteries

Saki Fukuma, Hikaru Sano, Moe Yamauchi, Keisuke Yasuda, Hisanori Ando, and Masaru Yao*

With the increasing demand for energy, the requirements for energy storage systems have also increased. For example, rechargeable lithium batteries, which are the primary power sources for mobile devices, must have a high energy density and be environmentally friendly. Herein, organic compounds linked by amide bonds that underwent chemical hydrolysis or biodegradation as sustainable battery materials are investigated. In particular, an amide-bonded anthraquinone oligomer is synthesized, and its potential as a cathode-active material is examined. The anthraquinone monomer, with a theoretical capacity of 258 mAh g^{-1}, exhibits rapid capacity decay during the cycle test; however, the synthesized oligomer, with a theoretical capacity of 144 mAh g^{-1}, exhibits excellent cycle-life performance. For example, it retains ≈82% of its initial capacity after 200 cycles. This electrochemical improvement is attributed to the decreased solubility in the electrolyte solution due to oligomerization. This study contributes to the development of long cycle-life organic batteries with environmental benefits.

1. Introduction

Recently, the use of mobile electronic devices, such as smartphones, tablets, laptop computers, and several other wireless devices, has increased, and numerous types of vehicles, including automobiles, aircraft, and ships, are being converted from coal power to electric power to achieve carbon-neutral societies. Rechargeable batteries serve as the primary power source for these devices and require a high energy density, long lifespan, thermal stability, recyclability, and low environmental burden. Conventionally, minor metal-based compounds have been used in the electrodes of lithium-ion batteries; however, their thermal stability is low, and recycling these metals from worn-out batteries remains challenging.[1,2] To address these requirements, we have investigated a series of redox-active organic compounds.[3,4] Organic batteries use organic electrode compounds and have attracted attention as next-generation energy storage systems owing to their lower cost, reduced weight, improved thermal stability, and minimal environmental impact.[5–16] To date, many organic electrode materials have been proposed, and among them, 9,10-anthraquinone (AQ) is an attractive model compound because of its good electrochemical reversibility and versatility in chemical modification. To realize a long cycle AQ-based compound, its oligomers and polymers have been suggested in which the AQ moieties are connected strongly via several types of chemical bonds such as ethylene unit,[17] thioether (—S—),[18] acetylene-based triple bond (—C≡C—),[19] and C—C bond via benzene or pyrazine ring.[20] These bonds are chemically stable and strong enough to provide high durability to these compounds; however, they become a hindrance in terms of recycling and biodegradation. We previously proposed the recycling of compatible and biodegradable organic electrode compounds, which were connected via amide bonds, that could undergo hydrolysis.[21] The synthesized amide-bond-connected anthraquinone (AQ) dimer and trimer showed a longer cycle life than that of the AQ monomer (**Figure 1**); however, their durability requires further improvement. To this issue, polymerization or oligomerization is considered an effective way.[22–26] In this study, we synthesized an extended AQ-based compound (oligomer) that demonstrated a longer cycle performance than those of the AQ monomer and the previously reported AQ dimer or trimer.

S. Fukuma, H. Sano, H. Ando, M. Yao
Department of Energy and Environment
National Institute of Advanced Industrial Science and Technology (AIST)
1-8-31 Midorigaoka, Ikeda, Osaka 563-8577, Japan
E-mail: m.yao@aist.go.jp

M. Yamauchi, K. Yasuda
Department of Applied Chemistry
Kobe City College of Technology (KCCT)
8-3 Gakuen-Higashimachi, Nishi-ku, Kobe 651-2194, Hyogo, Japan

Supporting information for this article is available on the WWW under https://doi.org/10.1002/batt.202500289

2. Results and Discussion

2.1. Materials Synthesis and Characterization

To synthesize the amide-bonded AQ multimer, a conventional condensation reaction between a carbonyl chloride and an amino group was performed according to a previously reported method.[21] 2,6-Diamino-AQ and terephthaloyl dichloride were heated in the presence of a base to obtain multimers

Research Article
doi.org/10.1002/batt.202500289
Chemistry Europe
European Chemical Societies Publishing

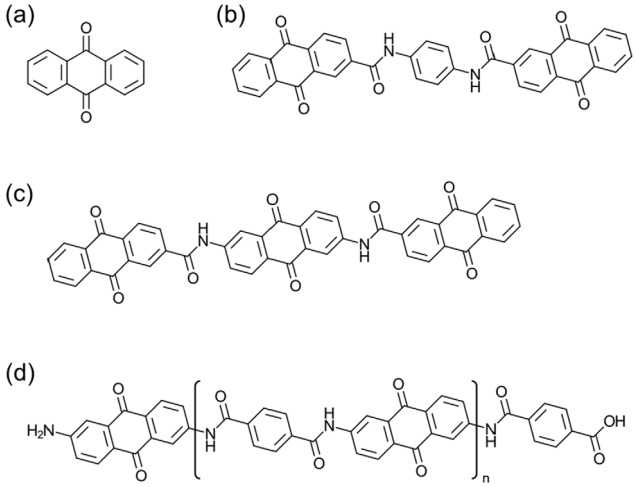

Figure 1. Structural formulas of AQ and its amide-bonded compounds: a) AQ monomer, b) dimer, c) trimer, and d) oligomer.

(**Figure 2**). Although the solubility of the newly synthesized compound in ordinary organic solvents was extremely low at room temperature, this insoluble property is preferable for realizing a long cycle-life active material. However, applying normal solution-based characterization techniques to such compounds remains challenging; therefore, other techniques used for solid analysis were employed to obtain structural information on the prepared compound.

SEM measurements of the synthesized compound were performed. The obtained powder comprised aggregated particles with relatively uniform size (**Figure 3**a). When magnified, the particles were ≈1 μm, and each particle presented as a film aggregate, implying low crystallinity (Figure 3b). Elemental analysis based on the EDX results showed that the synthesized compound comprised only C, N, and O. The absence of Cl, which was present in the raw material, implied that the desired condensation reaction proceeded (Figure 3c).

In general, gel permeation chromatography (GPC) and nuclear magnetic resonance (NMR) spectroscopy are often used to obtain information on the molecular weight of polymers; however, both techniques require high solubility in specific solvents. Owing to the low solubility of the obtained compound in ordinary solvents, these techniques could not be used in the present study. Therefore, XPS was employed as an alternative, although it is not commonly used in organic chemistry. Because XPS is a quantitative spectroscopy technique, it can be used to determine the molar mass by applying end-group analyses, which are typically used in ^{1}H-NMR spectroscopy. The XPS peaks in the C 1s region of the synthesized compound were divided into four peaks (**Figure 4**a). From low to high energy, the major peak at 284.8 eV was assigned to the C—C, C—N, and C—H bonds. The peaks at 286.6 and 287.8 eV were attributed to the >C═O bonds of the quinone skeletons and the —NHCO— bonds of the amide moieties, respectively. The broad peak at 289.9 eV reflects the π–π^* shake-up, which is often observed in aromatic compounds. The relative peak areas for >C═O and —NHCO— were similar (**Table 1**), confirming the structure of the synthesized compound shown in Figure 1d. The N 1s region was divided into two peaks at 398.2 and 400.0 eV, which were assigned to the terminal —NH_2 bonds and —NHCO—, respectively, suggesting the successful formation of amide bonds during synthesis (Figure 4b). The peak area comparison results indicated that the repeating number (*n*) was 3.5; therefore, the obtained compound was an AQ 4.5-mer (**Table 2**). Its average molar mass was ≈1,673 g mol^{-1}, which is much higher than those of the previously reported AQ dimer (576 g mol^{-1}), trimer (706 g mol^{-1}), and monomer (208 g mol^{-1}).

As a commonly used method for structural analysis, IR spectroscopy was performed. **Figure 5** compares the IR spectra of the AQ monomer and the synthesized oligomer. In the AQ spectrum,

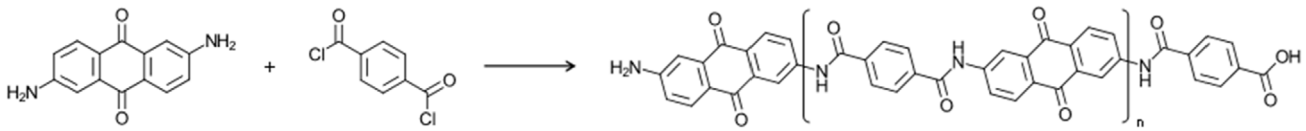

Figure 2. Synthesis of the amide-bonded AQ oligomer at 140 °C using *N,N*-diisopropylamine, xylene, and *N,N*-dimethylformamide.

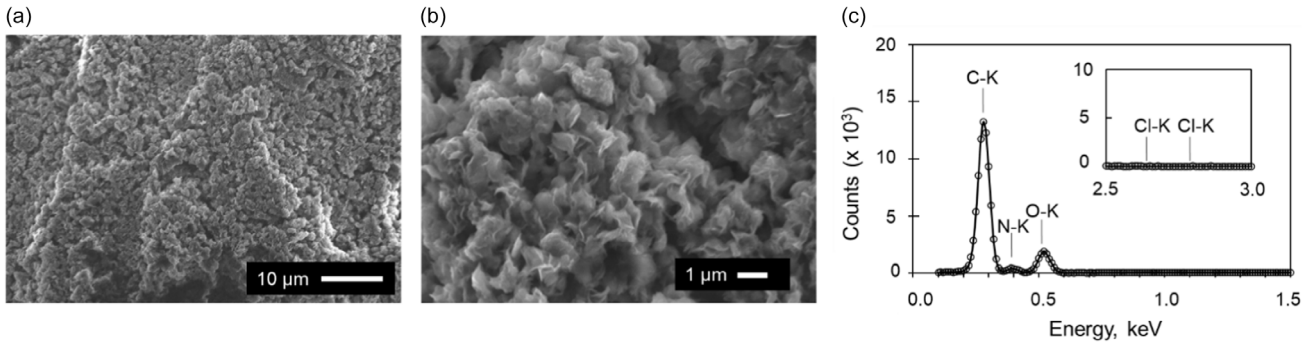

Figure 3. a)–b) SEM images of the AQ oligomer and c) EDX results.

Research Article
doi.org/10.1002/batt.202500289
Chemistry Europe
European Chemical Societies Publishing

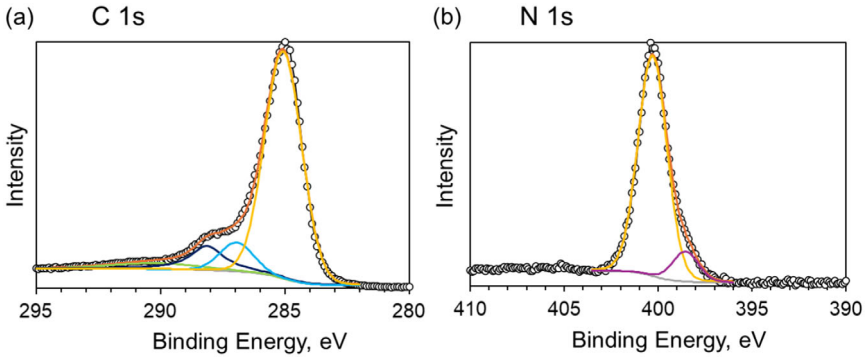

Figure 4. XPS spectra and curve fitting analysis of the AQ amide oligomer: profiles of the a) C 1s and b) N 1s nuclei were decomposed into a few peaks and Shirley background.

Table 1. XPS C 1s peak analysis of the oligomer. The peak attributions and relative area ratios were normalized with respect to the C═O peak area.

Peak position [eV]	Relative area ratio	Attribution
284.8	8.7	C—C, C—H, C—N
286.6	1.0	>C═O
287.8	1.2	—NHCO—
289.9	0.54	π–π^*

Table 2. XPS N 1s peak analysis of the oligomer. The peak attributions and relative area ratios were normalized to the —NH_2 peak area.

Peak position [eV]	Relative area ratio	Attribution
398.2	1.0	—NH_2
400.0	7.9	—NHCO—

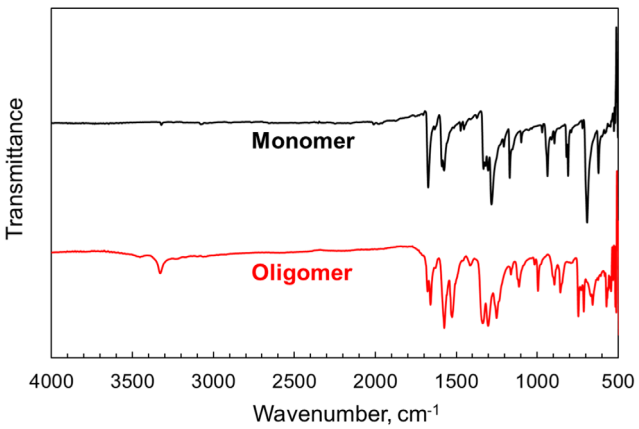

Figure 5. FTIR spectra of the AQ monomer and oligomer.

strong peaks at 1674 and 1578 cm^{-1} were attributed to the quinone stretching vibration and the C═C bond stretching vibration in the aromatic ring, respectively.[21] For the synthesized oligomer, two C═O stretching peaks at 1659 and 1677 cm^{-1} were observed. These two peaks correspond to amide and quinone bonds, respectively. The synthesized oligomer also exhibited a C═C bond peak at 1575 cm^{-1}. Furthermore, the synthesized oligomer showed an additional broad weak peak at ≈3328 cm^{-1}, which was attributed to the amide N—H bond. Peak splitting in the C═O stretching vibration region and emergence of the NH band were also observed in the spectra of the previously reported AQ dimer and trimer.[21] These observations confirmed the successful formation of amide bonds in the oligomer.

XRD was performed to obtain bulk structural information. Although the AQ monomer powder revealed numerous diffraction peaks, which reflected its high crystallinity, the AQ oligomer only exhibited broad peaks at $2\theta = 14°$ and 26° (**Figure 6**a), corresponding to distances of 6.2 and 3.4 Å, respectively. This result indicates that the degree of crystallinity decreased due to oligomerization. Notably, the distance of 3.4 Å was similar to that of typical π–π stacking, which is often observed in the crystals of aromatic compounds, including the AQ monomer (Figure 6b), and the interlayer distance of 3.4 Å for graphite. Therefore, this observation implies that the oligomer also has a π-stacked structure in the solid state. As for the lower angle peak at 14°, the AQ monomer also exhibited a peak at the same angle, reflecting the diffraction from the (1 0 $\bar{2}$) plane which corresponds to the minor axis distance of the AQ molecule (Figure 6c). This attribution provides an estimation that the oligomer powder also has a periodic structure in the minor axis direction, similar to the monomer. The absence of peaks in the region of angles less than 14° for the oligomer also suggests that the monomer units are bound in the major axis direction to build the oligomer, and there is a distribution in its length.

Because the AQ oligomer did not dissolve in ordinary solvents, a dissolution test in a battery electrolyte solvent was performed to examine its solubility in an actual battery system. **Figure 7**a shows the images of the dissolution analysis using diglyme as the electrolyte solvent. AQ was easily dissolved in diglyme, and the solution immediately became transparent. In contrast, diglyme did not dissolve the AQ oligomer. Instead, it exhibited a dispersed state after ultrasonication. After resting for one day, the dispersed powder precipitated, reflecting the density difference between the solvent and the oligomer. Subsequently, UV–vis spectroscopy was performed on the AQ solution and supernatant obtained from the oligomer dispersion. As shown in Figure 7b, a strong absorption band was observed at ≈250 nm, owing to the aromatic features of AQ. In contrast,

Research Article
doi.org/10.1002/batt.202500289
Chemistry Europe
European Chemical Societies Publishing

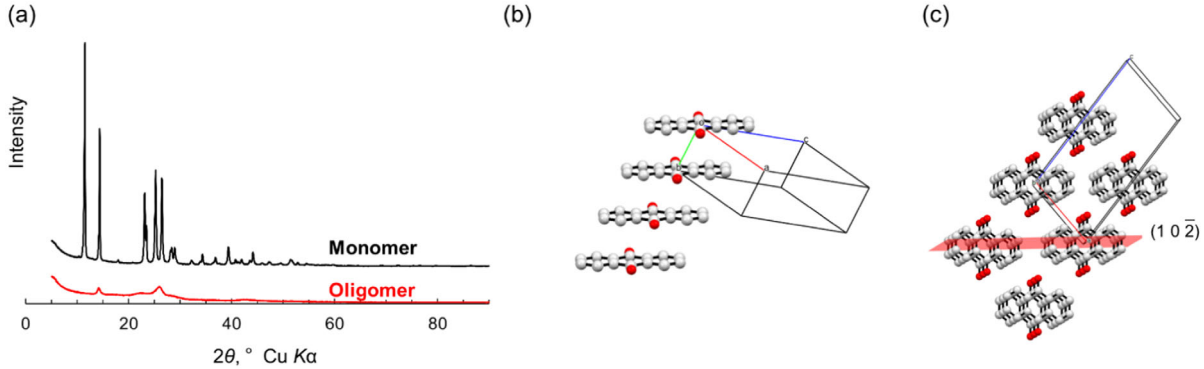

Figure 6. a) XRD patterns of the AQ monomer and oligomer. b) π-stacked columnar structure of the AQ monomer and c) the (1 0 $\bar{2}$) plane in the AQ monomer crystal. Crystal structures were depicted by using the reported data.[32]

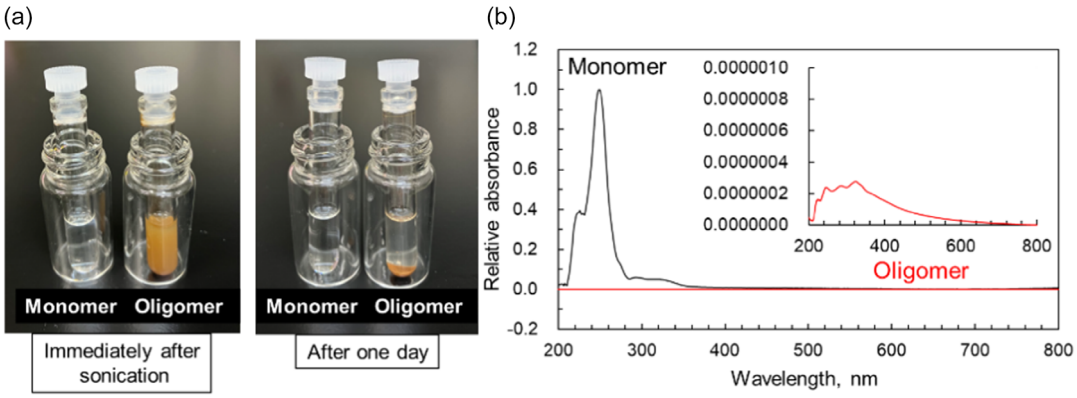

Figure 7. Dissolution test of the active materials in diglyme. a) Dispersion in the electrolyte solution after sonication and after one day. b) UV–vis spectra of AQ monomer and oligomer in diglyme. The dilution ratios of the oligomer supernatant and the diluted AQ solution were equal.

the supernatant liquid from the oligomer did not exhibit absorption bands in the entire wavelength region but exhibited extremely weak absorption bands in the UV region. These results indicate the extremely low solubility of the oligomer in diglyme.

DFT calculations were performed to predict the redox properties of the obtained oligomer. **Figure 8**a shows the optimized structure of an AQ oligomer, in which a pentamer ($n = 4$) was calculated to represent the synthesized oligomer ($n = 3.5$). The calculation yielded a roughly flat structure, although it exhibited a dihedral angle of ≈25° between the AQ units and adjacent terephthaloyl skeletons owing to steric hindrance. The calculated molecular orbitals of the pentamer are depicted in Figure 8b. The calculated energy levels of the unoccupied orbitals should correlate with the discharge voltage because electrons flow into these orbitals during the discharge (reduction) reaction. Moreover, the energy of the quinone center in the pentamer was split into several levels, reflecting the increased electronic interactions between the redox centers due to oligomerization. Therefore, the discharge curve in a practical measurement is predicted to follow a multistep process.

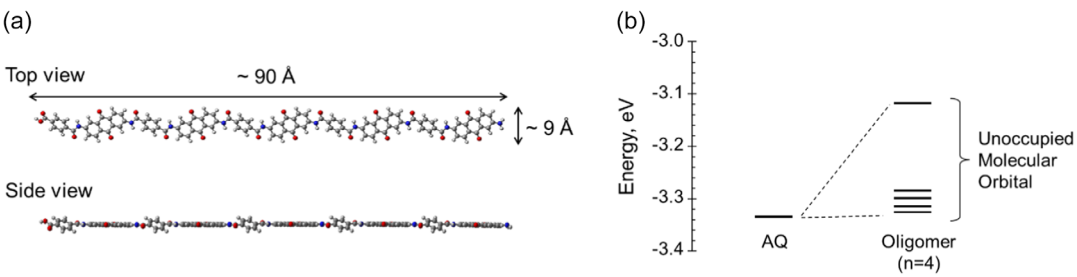

Figure 8. a) Optimized structure of an AQ oligomer model ($n = 4$) (C: gray, H: white, N: blue, O: red). b) Calculated energy levels of some molecular orbitals of the monomer and an oligomer model ($n = 4$). DFT (BLYP/6-31G(d)) was used for the computations. For the energy comparison, the optimized molecules placed in a cavity surrounded by a continuum medium were calculated to simulate their solid states.

Research Article
doi.org/10.1002/batt.202500289
Chemistry Europe
European Chemical Societies Publishing

2.2. Battery Performance

Figure 9a,b show the charge–discharge curves of AQ monomer and oligomer, respectively. The AQ monomer exhibited a high initial discharge capacity of 223 mAh g^{-1}, with a clear plateau voltage region at ≈2.3 V $Li_{C.E.}$. The calculated average voltage of 2.2 V versus $Li_{C.E.}$ was close to the plateau voltage, and the observed capacity corresponded to 79% of the theoretical value (258 mAh g^{-1}), where two-electron transfer per AQ unit was considered. In the subsequent first charge process, the AQ monomer exhibited a capacity of 169 mAh g^{-1}, which was lower than its initial discharge capacity. The charge–discharge capacity values rapidly decayed during cycling (Figure 9a), which is a common behavior for this compound. For the AQ oligomer shown in Figure 9b, the electrode exhibited a discharge capacity of 107 mAh g^{-1}, which was 73% of the theoretical value (144 mAh g^{-1}). Moreover, it exhibited a sloped discharge curve and an average voltage of 2.2 V $Li_{C.E.}$. The observed sloped voltage profile reflects the electronic interactions between the AQ sites in the oligomer. The above-mentioned DFT calculation showed that the energy levels of the molecular orbitals related to the discharge process were split by oligomerization. The observed phenomenon qualitatively agreed with the theoretical calculations. For the subsequent charge process, the initial charge capacity of 72 mAh g^{-1} was also lower than the initial discharge capacity, and the voltage profile showed a relatively large polarization. The difference between the charge and discharge capacities exhibited a decreasing trend, and the polarization decreased during cycling, probably due to structural relaxation and electrochemical activation by repeating ion insertion/deinsertion. In addition, the coulombic efficiency was almost 100% after ten cycles, and charge/discharge curves were similar, without any serious capacity degradation. **Figure 10**a,b show the trends in the actual capacity value (mAh g^{-1}) and retention (%), respectively. The oligomer had a lower theoretical capacity than the monomer and exhibited a lower actual initial discharge capacity; however, the capacity of the oligomer was higher than that of the monomer after ten cycles. For example, after 100 cycles, the monomer exhibited a capacity of only 22 mAh g^{-1} (retention of 11%), whereas the oligomer exhibited a capacity of 88 mAh g^{-1} (retention of 82%). After 200 cycles, the oligomer exhibited a capacity of 87 mAh g^{-1}. Thus, the oligomer exhibited an extremely stable cycle performance compared to that of the monomer. (The results of the rate capability test are shown in Figure S1–3 as supporting information.)

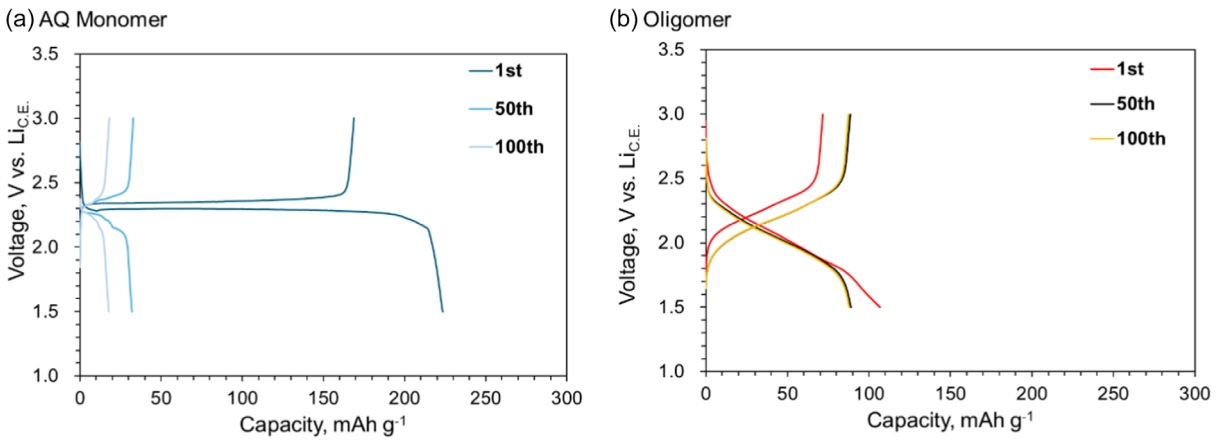

Figure 9. Charge–discharge curves of the electrodes using a) AQ monomer and b) oligomer.

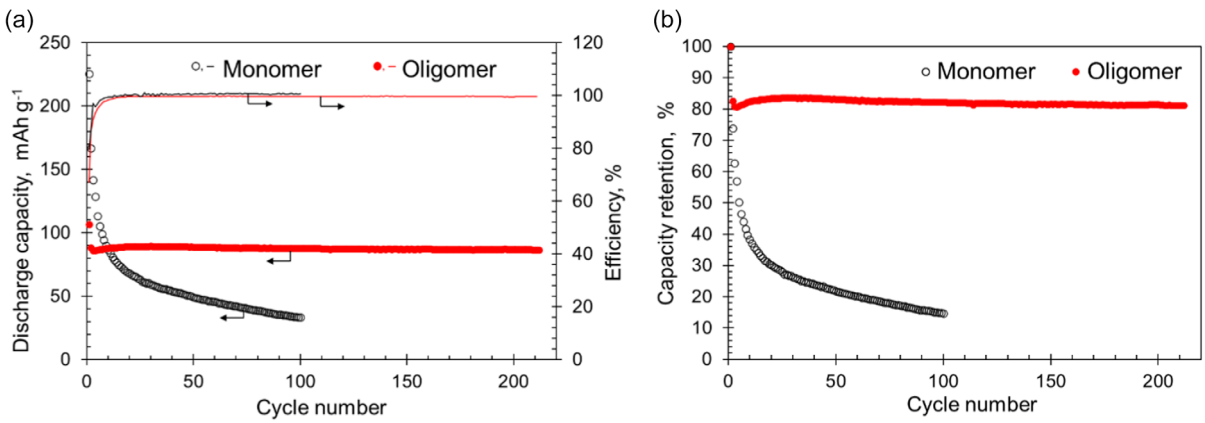

Figure 10. Cycle performance of the cells using the AQ monomer and the synthesized oligomer. a) Discharge capacity (mAh g^{-1}) and efficiency (ratio of charge to discharge in (%). b) Capacity and efficiency retention ratios relative to their initial values (%).

Table 3. Cyclic trends of the AQ monomer, dimer, trimer, and synthesized oligomer.

Materials	Theoretical capacity [mAh g^{-1}]	First discharge capacity [mAh g^{-1}]	100th discharge capacity [mAh g^{-1}]	Capacity retention [%]
Monomer	258	223[21]	22[21]	11[21]
Dimer	186	150[21]	47[21]	30[21]
Trimer	227	189[21]	82[21]	43[21]
Oligomer	144*	107	88	82

The theoretical capacity was calculated by assuming a 4.5-mer from the XPS results.

The AQ monomer is known for its poor cycle life, and one step of its degradation process involves the dissolution of the AQ molecule, which was evidenced by the color change of the electrolyte after the cycle test.[21] In contrast, the AQ oligomer exhibited a significantly improved cycling trend. Although the capacity decreased to ≈80% in the second cycle, it did not change after. We previously reported improved capacity retention for an amide-bonded dimer and trimer (Figure 1bc). **Table 3** summarizes the cycle trends of these compounds and the results of this study. The amide-bonded dimer showed a discharge capacity of 150 mAh g^{-1} during the first cycle, which subsequently decreased to 30% of its initial value after 100 cycles. The discharge capacity of the AQ trimer decreased to 43% after 100 cycles. The AQ oligomer synthesized in this study showed improved cycle performance compared to smaller compounds. Thus, the dissolution of organic compounds in the electrolyte solution during the charge–discharge process was significantly suppressed by oligomerization. Although the molar mass of the AQ-containing molecules could not be increased to the polymer level, the obtained oligomer exhibited sufficient cycle performance, indicating that polymerization is not always necessary to improve cycle characteristics. In our previous report,[21] we estimated the change in the solvation energy and attractive interaction between the AQ monomer, dimer, and trimer using DFT and found that the attractive interaction became stronger than the solvation energy when the molecular weight was increased. Although the compound synthesized in this study is an oligomer, not a polymer, it appears to have a sufficient molecular weight to overcome the solvation energy.

3. Conclusion

In this study, we successfully synthesized an AQ oligomer linked by amide bonds, which exhibited extremely low solubility in various organic solvents. Its structure was examined using various techniques suitable for solid analysis rather than the conventionally used solution-based characterization approaches. In particular, XPS revealed that the synthesized compound was an AQ-based tetramer or pentamer. This approach is useful for determining the molar mass of organic molecules that are insoluble in organic solvents. In battery tests, the AQ oligomer exhibited excellent cycle life performance. Although the theoretical capacity was lower than that of the AQ monomer owing to the redox-inactive heavy terephthaloyl linker, it could be improved by molecular modification.

Oligomers or polymers connected by amide bonds undergo hydrolysis and are easy to recycle. Considering their biodegradability, they have a low environmental burden. This type of molecular design concept should serve as an active material for future sustainable batteries.

4. Experimental Section

Materials

AQ (Kanto Chemical Co., Inc., Tokyo, Japan) and 2,6-diaminoanthraquinone (Tokyo Chemical Industry Co., Ltd., Tokyo, Japan), and terephthaloyl chloride (Tokyo Chemical Industry Co., Ltd., Tokyo, Japan) were used as received, without further purification.

Synthesis

To a dispersion of 2,6-diaminoanthraquinone (112 mg, 0.5 mmol) in a mixed dehydrated solvent of xylene (5 mL) and *N,N*-diisopropylamine (2.5 mL), a solution of terephthaloyl chloride (108 mg, 0.5 mmol) in dehydrated *N,N*-dimethylformamide (5 mL) was added at room temperature and heated at 140 °C overnight. After the dispersion cooled, the precipitate was filtered and washed to yield a yellow-brown powder that was insoluble in most of the solvents. Yield: 33 mg, 18%; MP: >400 °C; IR (cm^{-1}): 3328 (NH stretch), 1677, 1659 (C═O stretch), 1590, 1580 (aromatic ring stretch); XPS (eV): [C 1s] 284.8 (C—C, C—N, C—H) (calibration reference), 286.6 (C═O), 287.8 (NHCO), 289.9 (π–π^*); [N 1s], 398.2 (—NH_2), and 400.0 (NHCO).

SEM

SEM was conducted on the synthesized compound using a JSM-IT100 system (JEOL Ltd., Akishima, Tokyo, Japan) with an EDX probe (DrySD25, JEOL Ltd., Akishima, Japan).

XPS

XPS was conducted using a PHI 5000 VersaProbe (ULVAC-PHI, Chigasaki, Kanagawa, Japan) with a monochromatic Al-*Kα* X-ray (1486.6 eV) operated at a power and voltage of 25 W and 15 kV, respectively. The sample was first etched under spattering conditions of 1 kV for 1 min, which corresponded to a 1 nm min^{-1} sputter for SiO_2. The binding energies were referenced to the C 1s peak (284.8 eV) to account for the charging effects during the measurement. Peak fitting was performed using Gaussian–Lorentzian functions, and the background was subtracted using the Shirley method with XPSPeak 4.1.

FTIR Spectroscopy

To obtain information on the functional groups in the compounds, an FTIR spectrometer (Frontier FT-IR spectrometer, PerkinElmer, Inc., Waltham, MA, USA) equipped with an attenuated total reflection (ATR) stage was used for the powder samples.

UV–*vis Absorption Spectroscopy*

A UV–vis spectrophotometer (JASCO Corporation, Hachioji, Tokyo, Japan) was used to evaluate the dissolution of organic compounds. A quartz cuvette filled with diglyme solution (0.5 mL) was used. The AQ oligomer was dispersed at a concentration of

0.5 mg mL^{-1}, and the supernatant was assayed after 24 h. The AQ monomer was dissolved to 0.5 mg mL^{-1} and diluted 1600-fold for the assay.

XRD

To check the crystallinity of the compounds, XRD patterns were recorded using a RIGAKU Ultima IV X-ray diffractometer (Rigaku Corporation, Akishima, Tokyo, Japan) at 10° min^{-1}, 50 kV, and 40 mA. Samples were measured without grinding, and data were collected at $2\theta = 5°$–$90°$ using Cu–$K\alpha$ radiation with a scan speed of 1° min^{-1} and step size of 0.1°.

Quantum Chemistry Calculations

To estimate the structure and electrochemical properties of the monomer and oligomer, DFT-based calculations were performed with the 6-31 G (d) basis set and BLYP functional.[27,28] For the energy level calculation of the molecular orbitals, single-point calculations for the optimized structures using the polarizable continuum model[29] under a moderate dielectric constant ($\epsilon = 37$) were applied to imitate the solid-state environment surrounded by many polar functional groups. The Gaussian 16 program package was used with the graphical user interface of Gauss View 6.1.1.[30,31]

Cell Preparation

To examine the properties of the synthesized oligomers as positive electrode materials, a coin-type lithium metal half-cell was prepared. The organic compound powder, conductive additive (acetylene black), and binder (polytetrafluoroethylene) were mixed in a weight ratio of 4:5:1 to prepare a composite sheet containing 1.5 mg of the active material. Subsequently, the prepared composite was pressed onto a stainless-steel mesh-type current collector. The prepared positive electrode, lithium-metal negative electrode, and glass filter separator were assembled in the can of an IEC R2032 coin-type cell using an electrolyte solution (1 mol L^{-1} lithium bis(trifluoromethanesulfonyl)imide (LiTFSI)/diglyme) (0.2 mL).

Battery Measurements

A galvanostatic charge–discharge test at a current density of 20 mA g^{-1} was applied to the prepared coin-type cells in a voltage range of 1.5–3.0 V versus $Li_{C.E.}$ using a battery evaluation system (BLS series, Keisokuki Center Co., Ltd., Osaka, Japan and the ABE system, Electrofield Co., Ltd., Osaka, Japan). Measurements were performed at 30 °C.

Conflict of Interest

Authors declare no conflict of interest.

Data Availability Statement

The data that support the findings of this study are available from the corresponding author upon reasonable request.

Keywords: amide-bonded anthraquinones · biodegradability · oligomers · organic batteries · recycle

[1] P. Poizot, J. Gaubicher, S. Renault, L. Dubois, Y. Liang, Y. Yao, *Chem. Rev.* **2020**, *120*, 6490.
[2] G. Harper, R. Sommerville, E. Kendrick, L. Driscoll, P. Slater, R. Stolkin, A. Walton, P. Christensen, O. Heidrich, S. Lambert, A. Abbott, K. Ryder, L. Gaines, P. Anderson, *Nature* **2019**, *575*, 75.
[3] M. Yao, H. Ando, R. Kataoka, T. Kiyobayashi, N. Takeichi, *ECS Meet. Abstr.* **2016**.
[4] M. Yao, H. Senoh, S. Yamazaki, Z. Siroma, T. Sakai, K. Yasuda, *J. Power Sources* **2010**, *195*, 8336.
[5] P. Novák, K. Müller, K. S. V. Santhanam, O. Hass, *Chem. Rev.* **1997**, *97*, 207.
[6] K. Nakahara, S. Iwasa, M. Satoh, Y. Morioka, J. Iriyama, M. Suguro, E. Hasegawa, *Chem. Phys. Lett.* **2002**, *359*, 351.
[7] M. Armand, J. M. Tarascon, *Nature* **2008**, *451*, 652.
[8] T. Matsunaga, T. Kubota, T. Sugimoto, M. Satoh, *Chem. Lett.* **2011**, *40*, 750.
[9] Y. L. Liang, *Adv. Energy Mater.* **2012**, *2*, 742.
[10] N. Ogihara, T. Yasuda, Y. Kishida, T. Ohsuna, K. Miyamoto, N. Ohba, *Angew. Chem. Int. Ed.* **2014**, *126*, 11651–.
[11] S. Muench, A. Wild, C. Friebe, B. Häupler, T. Janoschka, U. S. Schubert, *Chem. Rev.* **2016**, *116*, 9438.
[12] Y. Liang, Z. Chen, Y. Jing, Y. Rong, A. Facchetti, Y. Yao, *J. Am. Chem. Soc.* **2015**, *137*, 4956.
[13] S. Natarajan, V. Aravindan, *ACS Energy Lett.* **2018**, *3*, 2101.
[14] J. Yang, H. Su, Z. Wang, P. Sun, Y. Xu, *ChemSusChem* **2020**, *13*, 2436.
[15] K. Hashimoto, T. Hamano, M. Okada, *J. Appl. Polym. Sci.* **1994**, *54*, 1579.
[16] F. B. Oppermann, S. Pickartz, A. K. Steinbüchel, *Polym. Degrad. Stabil.* **1998**, *59*, 337.
[17] W. Choi, D. Harada, K. Oyaizu, H. Nishide, *J. Am. Chem. Soc.* **2011**, *133*, 19839.
[18] Z. Song, Y. Qian, M. L. Gordin, D. Tang, T. Xu, M. Otani, H. Zhan, H. Zhou, D. Wang, *Angew. Chem. Int. Ed.* **2015**, *54*, 13947.
[19] M. Yao, H. Sano, H. Ando, T. Kiyobayashi, N. Takeichi, *ChemPhysChem.* **2019**, *20*, 967.
[20] H. Yu, S. Li, J. Yang, Y. Xu, Y. Li, *Chem. Eng. J.* **2023**, *466*, 143316.
[21] M. Yao, H. Sano, H. Ando, *Polymers* **2023**, *15*, 4395.
[22] Z. Song, H. Zhan, Y. M. Zhou, *Chem. Commun* **2009**, *4*, 448.
[23] T. Nokami, T. Matsuo, Y. Inatomi, N. Hojo, T. Tsukagoshi, H. Yoshizawa, A. Shimizu, H. Kuramoto, K. Komae, H. Tsuyama, J. Yoshida, *J. Am. Chem. Soc.* **2012**, *134*, 19694-19700.
[24] Y. Jing, Y. Liang, S. Gheytani, Y. Yao, *Nano Energy* **2017**, *37*, 46.
[25] T. Yokoji, Y. Kameyama, *J. Mater. Chem. A* **2016**, *4*, 5457.
[26] Y. Inatomi, N. Hojo, T. Yamamoto, S. Watanabe, Y. Misaki, *ChemPlusChem.* **2012**, *77*, 973.
[27] A. D. Becke, *Phys. Rev.* **1988**, *A38*, 3098.
[28] C. Lee, W. Yang, R. G. Parr, *Phys. Rev.* **1988**, *B37*, 785.
[29] S. Miertuš, E. Scrocco, J. Tomasi, *Chem. Phys.* **1981**, *55*, 117.
[30] M. J. Frisch, G. W. Trucks, H. B. Schlegel, G. E. Scuseria, M. A. Robb, J. R. Cheeseman, G. Scalmani, V. Barone, G. A. Petersson, H. Nakatsuji, X. Li, M. Caricato, A. V. Marenich, J. Bloino, B. G. Janesko, R. Gomperts, B. Mennucci, H. P. Hratchian, J. V. Ortiz, A. F. Izmaylov, J. L. Sonnenberg, D. Williams-Young, F. Ding, F. Lipparini, F. Egidi, J. Goings, B. Peng, A. Petrone, T. Henderson, D. Ranasinghe et al., *Gaussian 16, Revision C.01*, Gaussian, Inc., Wallingford, UK, **2016**.
[31] R. Dennington, T. Keith, C. Millam, J. Gauss, *Version 6.1.1*, Semichem Inc., Shawnee Mission, KS, USA, **2016**.
[32] M. Slouf, *J. Mol. Struct.* **2002**, *611*, 139.

Manuscript received: April 18, 2025
Revised manuscript received: June 11, 2025
Version of record online: